EMITTANCE MEASUREMENT OF THE CERN ANTIMATTER BEAM WITH THE GBAR EXPERIMENT

S. Geffroy*, CNRS/IN2P3, IJCLab, Orsay (France) and the GBAR Collaboration†

Abstract

Emittance measurements were performed for the antiproton and H^- beams delivered by the AD/ELENA facility at CERN, with and without the deceleration stage of the GBAR experiment. The measurements rely on a quadrupole-scan technique using a cylindrically symmetric Einzel lens, with beam-spot imaging on a microchannel plate coupled to a phosphor screen. Transport coefficients are obtained from SIMION particle tracking simulations. For the 100 keV H^- beam, the normalized emittance is found to increase with bunch intensity, ranging from 0.025 to 0.039 mm·mrad in the vertical plane and 0.035 to 0.052 mm·mrad in the horizontal plane. After deceleration to 6 keV, a significant growth of the projected normalized emittance is observed, substantially exceeding the values predicted by SIMION simulations accounting for energy dispersion alone. RF-Track simulations indicate that this growth results from non-linear aberrations induced by the Einzel lens, amplified by space-charge effects. These results provide updated beam models that better match the measured transport efficiencies through GBAR.

INTRODUCTION

The GBAR (Gravitational Behaviour of Antihydrogen at Rest) experiment [1] is located at the CERN Antimatter Factory [2]. Its goal is to measure the free fall of ultra-cold antihydrogen atoms in the Earth's gravitational field. Unlike other antihydrogen experiments, GBAR will produce antihydrogen *ions* ($\overline{H}^+$), which can be sympathetically cooled to the microkelvin range. The production of $\overline{H}^+$ requires two successive charge-exchange reactions occurring within a small interaction region where an antiproton beam overlaps with a positronium (Ps) cloud:

$$\bar{p} + \mathrm{Ps} \rightarrow \overline{H} + e^-, \tag{1}$$

$$\overline{H} + \mathrm{Ps} \rightarrow \overline{H}^+ + e^-. \tag{2}$$

Part of the AD complex at CERN, the Extra-Low Energy Antiproton (ELENA) ring delivers antiproton bunches with a kinetic energy of 100 keV every two minutes and 100 keV H^- bunches every 15 seconds.

The optimal antiproton energy for the double charge-exchange reaction with ground-state positronium is 6 keV [3]. The antiproton beam is therefore decelerated from 100 keV to 6 keV using a 450 mm long drift tube held at -94 kV and pulsed to ground while the beam bunch is inside [4]. While the normalized emittance $\varepsilon_n = \beta\gamma\,\varepsilon_{\mathrm{geo}}$ remains conserved under deceleration, the geometric emittance $\varepsilon_{\mathrm{geo}}$ increases by a factor $\sqrt{100/6} \simeq 4$.

In 2022, the GBAR experiment observed the first production of antihydrogen atoms via the first charge-exchange reaction [1]. However, the measured production rate was limited by both the positronium density and the fraction of antiprotons delivered within the interaction region. To increase this rate, two upgrades were implemented. First, a positronium production cavity was installed, providing a significantly higher positronium density within the interaction volume. Second, a Penning–Malmberg trap was installed on the antiproton beam line upstream of the interaction region [5]. Antiprotons are accumulated and cooled in this trap through Coulomb interactions with a cold electron plasma, reducing the transverse emittance of the $\bar{p}$ beam before extraction and reacceleration to 6 keV for transport through the Ps cavity. The optics for injecting the decelerated antiproton beam into the trap were designed taking into account the expected emittance growth from deceleration. However, experimental measurements yield an injection efficiency of only about 70%. To understand this discrepancy, a measurement of the emittance of both the non-decelerated and decelerated beams was performed.

METHOD

We used the classical quadrupole-scan method [6] with a cylindrically symmetric uni-potential lens, measuring the beam-spot size with a standard microchannel-plate/phosphor-screen imaging system. An example is shown in Fig. 1. The transverse beam sizes are extracted from MCP images by analyzing the intensity distribution on the phosphor screen. A dark image is subtracted to remove background, and a fixed region of interest centered on the MCP is selected.

The transport coefficients necessary for determining the emittance are obtained using the electromagnetic modeling and charged particle tracking software SIMION. Figure 2 illustrates a SIMION model of the electrostatic beam elements used in this study. For each Einzel lens voltage, the linear transport coefficients M_{11} and M_{12} between the reconstruction point and the MCP are determined by tracking test particles with controlled initial conditions. A particle

* sarah.geffroy@ijclab.in2p3.fr

† GBAR Collaboration: P. Adrich (NCBJ), I. Belosevic (IRFU), M. Chung (POSTECH), P. Cladé (LKB), P. Comini (IRFU), D. Cotte (IRFU), P. Crivelli (ETHZ), P. Debu (IRFU), A. Douillet (LKB), S. Geffroy (U. Paris-Saclay), S. Guellati (LKB), P.-A. Hervieux (ICPMS), L. Hilico (LKB), P. Indelicato (LKB), S. Jonsell (Stockholm U.), J-P. Karr (LKB), B. Kim (IBS), S. Kim (SNU), E-S. Kim (Korea U.), N. Kuroda (U. Tokyo), B. Lee (SNU), L. Liszkay (IRFU), D. Lunney (CNRS-IN2P3), G. Manfredi (ICPMS), B. Mansoulié (IRFU), M. Matusiak (NCBJ), V. Nesvizhevsky (ILL), F. Nez (LKB), K. Park (SNU), E. Perez (CERN), P. Pérez (IRFU), C. Regenfus (ETHZ), J-Y. Roussé (IRFU), F. Schmidt-Kaler (Uni-Mainz), K. Szymczyk (NCBJ), F. Tano (U. Tokyo), B. Tuchming (IRFU), D.-P. van der Werf (Swansea U.), D. Won (SNU), S. Wronka (NCBJ), K-H. Yoo (POSTECH), P. Yzombard (LKB)

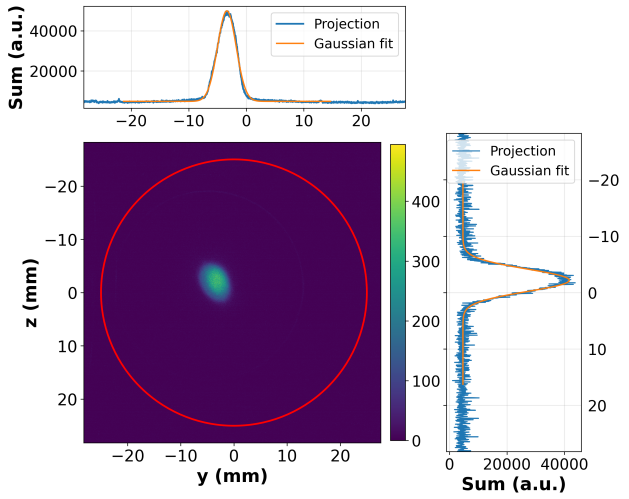

Figure 1: Beam spot obtained on a MCP detector with phosphor screen for a 100 keV H^- beam. The signal is projected onto the horizontal (y) and vertical (z) axes, and the resulting profiles are fitted with Gaussian functions (with constant offset), yielding beam sizes σ_y and σ_z.

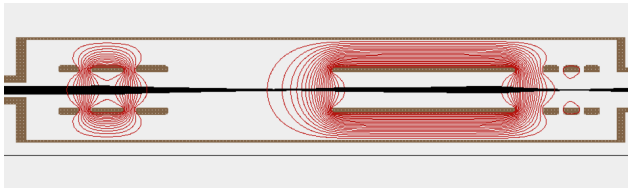

Figure 2: SIMION optical model of the GBAR decelerator, showing equipotentials and antiproton trajectories. All electrodes have cylindrical symmetry and an inner diameter of 100 mm. The ELENA beam enters from the left, is focused by the first Einzel lens and can be decelerated by the long drift tube held at -94 kV that is switched to ground while the 300 ns (rms) bunch is inside [4] and refocused with the second Einzel lens. The MCP-PS is located 265 mm downstream.

launched with $x_0 \neq 0$ and $x_0' = 0$ yields $M_{11} = x/x_0$, while a particle with $x_0 = 0$ and $x_0' \neq 0$ gives $M_{12} = x/x_0'$. The measured beam size contains both betatron and dispersive contributions, given by:

$$D_{\mathrm{MCP}} = M_{11} D_0 + M_{12} D_0' + D_{\mathrm{SIMION}} \tag{3}$$

where D_0 and D_0' are the dispersion coefficients given by ELENA at the entrance of the GBAR beamline and D_{SIMION} is obtained numerically by tracking particles with small momentum offsets $\delta = \Delta p/p$ between the entrance of the beamline and the MCP used for the scan. The dispersive contribution $(D_{\mathrm{MCP}}\,\sigma_\delta)^2$ is subtracted from the measured beam size, so that the betatron component

$$\sigma_\beta^2 = \sigma_x^2 - (D_{\mathrm{MCP}}\,\sigma_\delta)^2 \tag{4}$$

is used in the fit. By varying the lens voltage, the resulting beam sizes σ_β^2 are fit using

$$\sigma_\beta^2 = M_{11}^2 \langle x_0^2 \rangle + 2 M_{11} M_{12} \langle x_0 x_0' \rangle + M_{12}^2 \langle x_0'^2 \rangle. \tag{5}$$

The second-order moments are obtained from a least-squares fit, and the geometric emittance is given by

$$\varepsilon_{x,\mathrm{rms}} = \sqrt{\langle x_0^2 \rangle \langle x_0'^2 \rangle - \langle x_0 x_0' \rangle^2}. \tag{6}$$

RESULTS

100 keV H^- Beam

The drift tube, normally used to decelerate the beam, is set to 0 V. The voltage applied to the first Einzel lens of the GBAR beam line (Fig. 2, left) is varied, while all other optical elements are kept at ground. Due to large shot-to-shot H^- intensity fluctuations, 15 shots are recorded for each voltage setting. The data are grouped according to beam intensity, and the transverse beam size is extracted for each focusing voltage, as shown in Fig. 3.

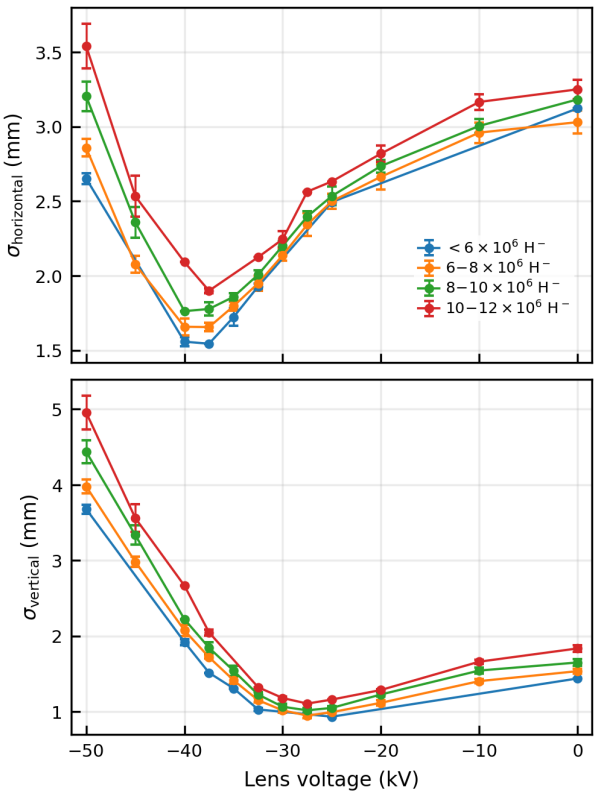

Figure 3: Transverse beam size as a function of the Einzel lens voltage for a 100 keV H^- beam. The data are grouped by beam intensity. Each point is an average over 15 shots.

For each intensity bin, the normalized transverse emittance is estimated at the reconstruction point. The results are shown in Fig. 4. These values can be compared to the normalized emittances measured at the source by the ELENA operators: $\varepsilon_{n,\mathrm{hor}} = 0.16$ mm · mrad and $\varepsilon_{n,\mathrm{vert}} = 0.097$ mm · mrad (r.m.s., reconstructed at the H^- source) [7]. They are larger than our full-intensity measurement by a factor of three, which is expected since they characterize the beam before transport through the ELENA ring and transfer line.

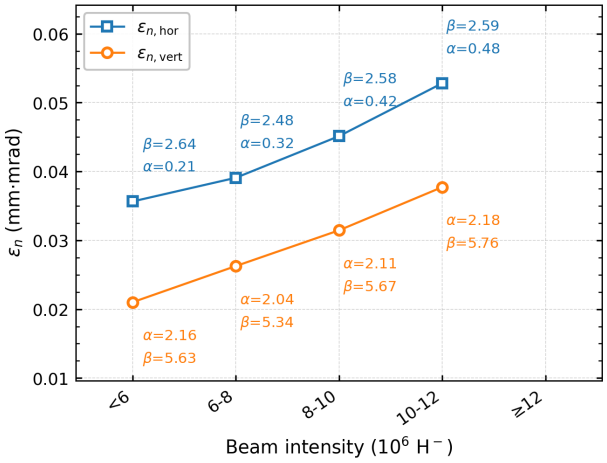

Figure 4: Normalized transverse emittances as a function of the beam intensity for a 100 keV H$^-$ beam. The emittance is reconstructed from beam size measurements after correction of the dispersive contribution.

To validate the consistency of these results, we simulate the beam generated from the emittance results obtained above (for the case of 8-10 × 10^6) using two different ion-optics codes, RF-Track [8] and Simion. For each value of the scanning voltage V_1, the transverse beam size σ is extracted at the measurement plane and compared with the experimental data points obtained, as shown in Fig. 5. The two simulations give accurate and consistent results for the measured beam sizes.

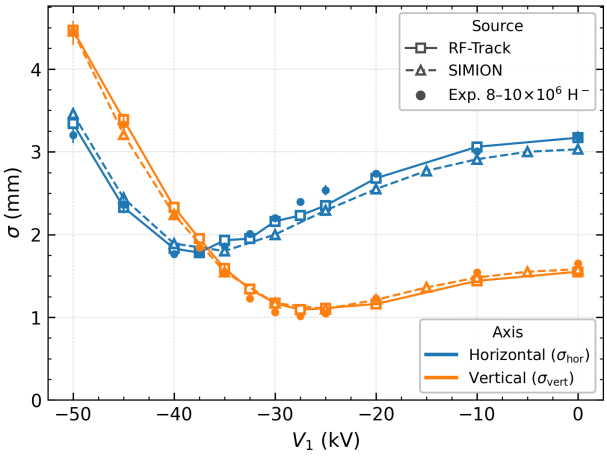

Figure 5: Comparison between measured and simulated transverse beam sizes as a function of the Einzel lens voltage for a 100 keV beam of intensity 8 – 10 × 10^6.

H$^-$ Beam Decelerated to 6 keV

The H$^-$ beam is decelerated by the pulsed drift tube and focused with the downstream low-voltage lens (Fig. 2, right). The variation of the transverse beam size as a function of focussing voltage is shown in Fig. 6. The measured beam sizes are systematically larger than those expected from the increase in geometric emittance resulting from the change in energy. They are also larger than those predicted by Simion

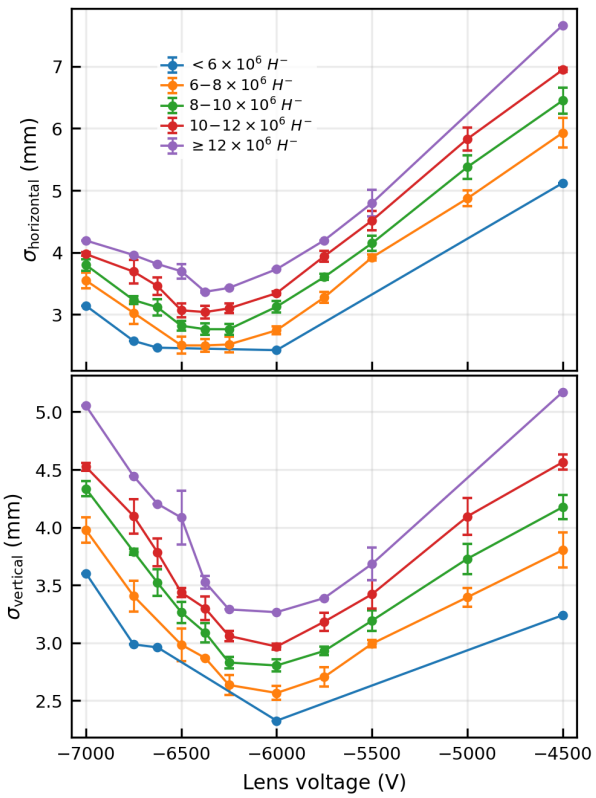

Figure 6: Transverse beam size as a function of the lens voltage for a 6 keV H$^-$ beam. The drift tube is pulsed from -94 kV to 0V while the bunch is inside. The data are grouped by beam intensity.

and moreover, yield emittance values that depend on focussing voltage. Given the effective current of 10^7 charged particles within 300 ns decelerated to such low energies, it seems plausible that space charge plays a role in the beam dynamics.

The Simion simulations include the effect of energy dispersion but not the effects of space charge.

Therefore, a more detailed simulation was made using RF-Track [8] to understand the effects of energy dispersion, space charge and the normalized emittance growth.

In RF-Track, the beam is tracked through the electrostatic elements using field maps generated with COMSOL and a user-defined pulsed drift-tube model. The input beam parameters are those found for the 100 keV beam that yield the consistence results shown in Fig. 5. At the MCP position, the full transverse phase space is extracted to evaluate the beam size, the mean kinetic energy, the local dispersion, and two different emittance definitions, the projected emittance (assuming no energy-dispersion contribution) and the betatronic emittance. The projected emittance is obtained directly from the full transverse phase-space distribution (x, x') or (y, y'). It therefore includes both the intrinsic betatron contribution and the broadening induced by momentum spread through dispersion. In addition, a local betatron emittance is reconstructed by removing the linear dispersive contribution from the transverse coordinates and angles. Local dispersions

D_x, D'_x, D_y, and D'_y are estimated from the correlations with the relative momentum deviation $\delta = (P - \langle P \rangle)/\langle P \rangle$. The betatron coordinates are then defined as

$$x_\beta = x - D_x\delta, \qquad x'_\beta = x' - D'_x\delta,$$

$$y_\beta = y - D_y\delta, \qquad y'_\beta = y' - D'_y\delta.$$

The transverse beam size for a beam intensity of 8–10 × 10^6 H^- at the measurement plane is compared with the experimental data and the SIMION predictions in Fig. 7.

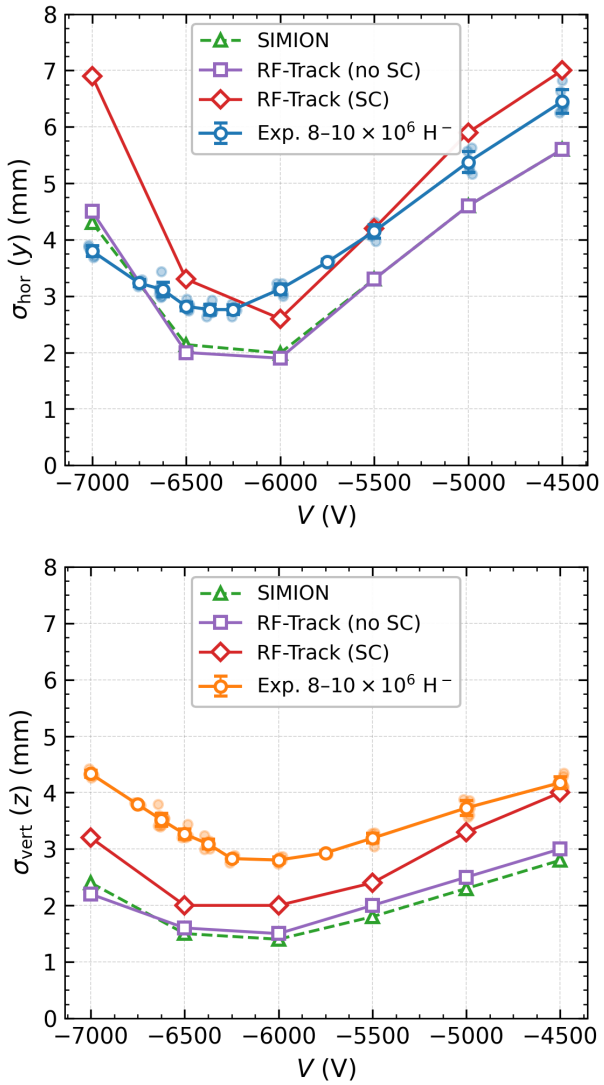

Figure 7: Transverse beam size as a function of the einzel lens voltage for a 6 keV H^- beam at an intensity of 8–10 × 10^6 H^-, for the horizontal (top) and vertical (bottom) planes. Experimental data are compared with SIMION and RF-Track simulations with and without space charge. Faded markers indicate the experimental points used.

The r.m.s. emittance of the decelerated beam is sensitive to the einzel lens voltage, as the lens introduces spherical aberrations that drive emittance growth. Space-charge forces are also non-negligible at this intensity and contribute an additional emittance increase. The evolution of the emittance with respect to the voltage applied on the Einzel lens is shown in Fig. 8.

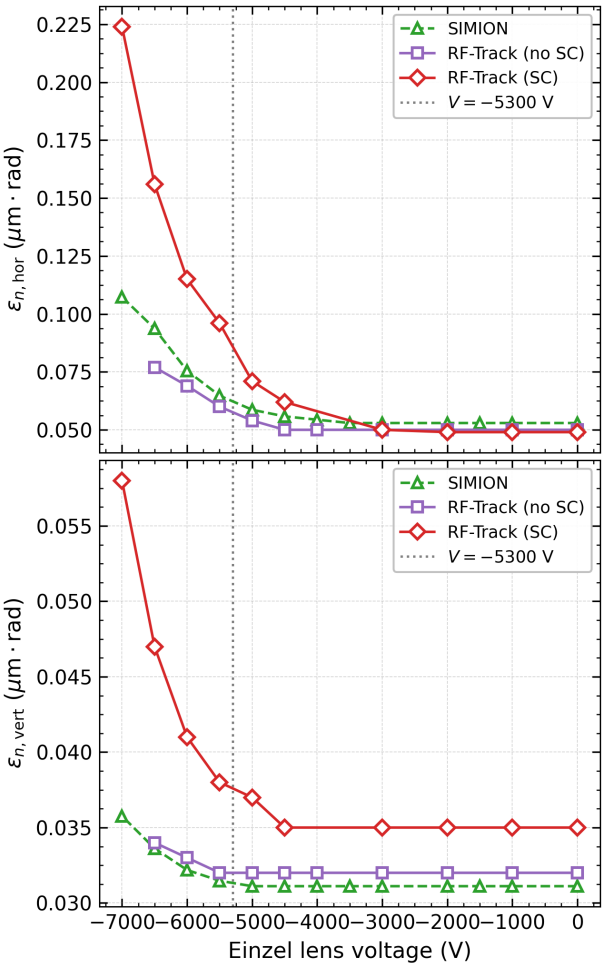

Figure 8: Normalized r.m.s. emittance as a function of the einzel lens voltage for a 6 keV H^- beam, for the horizontal (top) and vertical (bottom) planes. Results from SIMION and RF-Track simulations with and without space charge are compared. The dotted vertical line indicates the nominal operating voltage $V = -5.3$ kV.

$\bar{p}$ beam decelerated to 6 keV The voltage scan was performed following the same procedure as for the H^- beam. The voltage scan is shown in Fig. 9. For the 6 keV $\bar{p}$ beam, all shots exhibit a stable intensity, ranging from 11.5 × 10^6 to 13.5 × 10^6 antiprotons per bunch, therefore no intensity classification was made.

The voltage scan results closely match those measured for the H^- beam at an intensity of 10–12 million particles. However, different effects are expected. First, the antiproton beam contains a larger number of particles, leading to stronger space-charge. Second, the response of antiprotons on a microchannel plate (MCP) coupled to a phosphor screen is known to be artificially enlarged due to pion production following antiproton annihilation on the detector surface [9]. For these reasons, the emittance of the antiproton beam

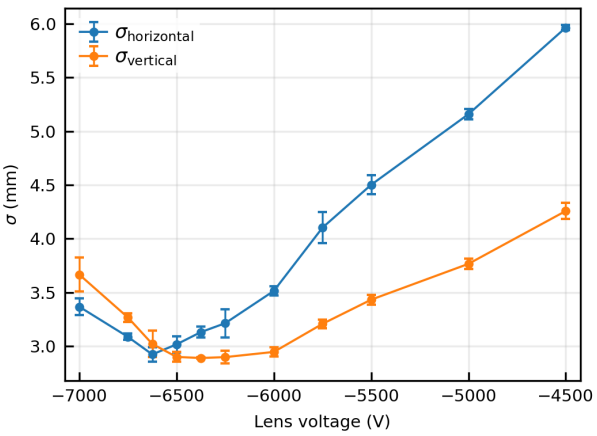

Figure 9: Voltage scan for the 6 keV antiproton beam. The beam-spot size as a function of the Einzel lens voltage is used to extract the projected normalized emittance.

should be regarded as an upper limit, consistent with that of the H^- beam at 10–12 million particles.

CONCLUSIONS

Emittance measurements of the AD/ELENA beams provided by CERN's "Antimatter Factory" were carried out using instruments in the GBAR experiment that can also decelerate the nominally 100 keV ELENA beam. Results for the 100 keV H^- are consistent with measurements by the ELENA group, however the emittances of the decelerated H^- and antiproton beams are significantly larger than can be accounted for by the relative energies. A detailed simulation using the CERN software RF-Track was performed to evaluate the contributions of space charge, which turn out to contribute significantly to larger emittances when decelerating and strongly focussing the intense ELENA beams. While GBAR has demonstrated 100% efficiency with its pioneering deceleration technique compared to thin foils used by other experiments, the effects of space charge require refining the ion optics for transport and injection into traps.

REFERENCES

[1] P. Adrich *et al.*, "Production of antihydrogen atoms by 6 keV antiprotons in a positronium cloud," *Eur. Phys. J. C*, vol. 83, p. 1004, 2023. doi:10.1140/epjc/s10052-023-12137-y

[2] C. Carli, D. Gamba, C. Malbrunot, L. Ponce, and S. Ulmer, "ELENA: bright perspectives for low energy antiproton physics," *Nucl. Phys. News*, vol. 32, pp. 21–26, 2022. doi:10.1080/10619127.2022.2100646

[3] P. Comini and P. A. Hervieux, "$\bar{H}^+$ ion production from collisions between antiprotons and excited positronium: cross sections calculations in the framework of the GBAR experiment," *New J. Phys.*, vol. 15, p. 095022, 2013. doi:10.1088/1367-2630/15/9/095022

[4] A. Husson *et al.*, "A pulsed high-voltage decelerator system to deliver low-energy antiprotons," *Nucl. Instrum. Methods Phys. Res. A*, vol. 1002, p. 165245, 2021. doi:10.1016/j.nima.2021.165245

[5] B. Lee *et al.*, "Record accumulation of antiprotons in a Penning–Malmberg trap and their preparation for improved production of antihydrogen beams," 2026. doi:10.48550/arXiv.2603.21168

[6] J. Kallestrup, M. Aiba, N. Carmignani, and T. P. Perron, "A dispersive quadrupole scan technique for transverse beam characterization," in *Proc. IPAC'21*, Campinas, Brazil, May 2021, pp. 107–110. doi:10.18429/JACoW-IPAC2021-MOPAB021

[7] L. Bojtar, V. Bencini, and Y. Dutheil, "H^- source characterization and transfer line studies with realistic EM fields in the ELENA decelerator at CERN," in *Proc. IPAC'24*, Nashville, TN, USA, May 2024, pp. 2616–2618. doi:10.18429/JACoW-IPAC2024-WEPR53

[8] A. Latina, "The tracking code RF-Track and its application," in *Proc. HB'23*, Geneva, Switzerland, Oct. 2023, pp. 245–248. doi:10.18429/JACoW-HB2023-WEA3C1

[9] G. B. Andresen *et al.*, "Antiproton, positron, and electron imaging with a microchannel plate/phosphor detector," *Rev. Sci. Instrum.*, vol. 80, p. 123701, 2009. doi:10.1063/1.3266967